Earth, Planets and Space

FULL PAPER Open Access

Azimuthal differences and changes in strain rate and stress of the Japanese Islands deduced from geophysical data

Issei Kosugi and Yuta Mitsui*

Abstract

Geodetic and seismological observations have shown discrepancies between azimuths of maximum contraction (strain rate) and maximum compression (stress). These discrepancies can be the results of the superposition of localized or transient mechanical processes such as fault coupling during seismic cycles. Rich sets of recent geophysical data allow us to conduct spatiotemporal imaging of the discrepancies. Here, we estimate the spatiotemporal evolution in the strain-rate fields of the Japanese Islands with optimized smoothing distances from 1997 to 2021 using Global Navigation Satellite System (GNSS) data, and investigate how the maximum contraction axes of horizontal strain rates differ from those of horizontal stress based on earthquake focal mechanisms. Several characteristic results are observed for each region within the Japanese Islands. Both azimuths of the strain rates and stress differ by more than 60° over hundreds of kilometers from the Kanto region to along the Nankai Trough, related to seismotectonics due to the dual subduction of the Philippine Sea plate and the Pacific plate beneath the Japanese Islands. The differences in the azimuths imply the effect of the very long-term stable subduction of the Pacific plate. We find that the azimuthal differences tend to be small along tectonic zones with active inland earthquakes and high strain rates on the back-arc sides. We also find that the 2011 off the Pacific coast of Tohoku earthquake caused notable azimuthal differences in the strain rates and the stress in the Tohoku region. The strength of fault may cause lower response sensitivity of seismological stress to major earthquakes than geodetic strain rate. Our dataset has wide spatiotemporal coverage and can serve as a basis for further research, for example, to estimate the current fault conditions during seismic cycles.

Keywords: GNSS, Strain rate, Earthquake focal mechanism, Stress, Contraction azimuth, Subduction zone, Tectonic zone

*Correspondence: mit@shizuoka.ac.jp

Department of Geosciences, Shizuoka University, 836, Ohya, Suruga-ku, Shizuoka 422-8529, Japan

Graphical Abstract

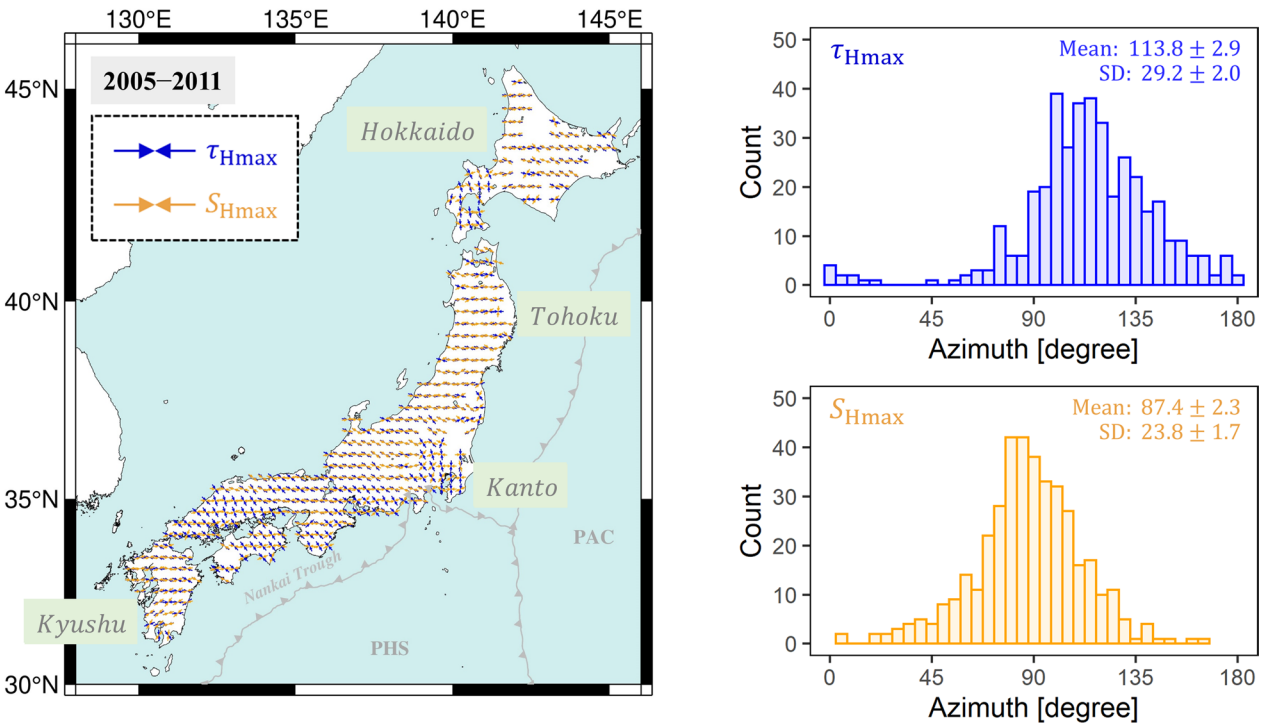

Introduction

In elementary elastomechanics, strain and stress are proportional through elastic constants, and thus the strain and stress fields are similar. However, there are frequent discrepancies between the strain field estimated from geodetic observations (strain rate field) and the stress field estimated from seismological observations.

A pioneering study (Sbar 1983) cited an example where the azimuth of the principal strain rate from geodetic data was far different from the azimuth of the principal stress from earthquake data. They interpreted this difference that geodetic strain rates reflect temporal deformation during observation periods, whereas earthquakes reflect averages of longer durations. In another study (Wang 2000) for the Nankai Trough, southwestern Japan, and the Cascadia subduction zones, the geodetic strain rates indicated contraction in the direction of plate convergence, while the seismological stress showed maximum compression along strike. They called the phenomenon a stress–strain 'paradox' and modeled the forearc stress regime.

A recent study (Townend and Zoback 2006) examined how the azimuths of geodetic principal strain rates based on Global Navigation Satellite System (GNSS) data differed from the azimuths of principal stress based on earthquake focal mechanisms in central Japan. The azimuths of the maximum contraction of the geodetic strain-rate fields corresponded to the azimuths of the maximum compressive stress after removing the effect of elastic strain due to the subduction megathrust locking (which will be released by megathrust earthquakes) at the Nankai Trough (Mazzotti et al. 2000; Henry et al. 2001). These azimuths were interpreted to be the long-term horizontal motion between northeastern and southwestern Japan representing the mountain-building collision processes (Heki and Miyazaki 2001; Mazzotti et al. 2001). Another study (Matsumoto et al. 2015) also compared the azimuths of geodetic principal strain rates and seismological principal stress and confirmed their consistency for the Kyushu region (south of about 34° N and west of about 132° E), southwestern Japan.

The strain-rate and stress fields would coincide under a sufficiently long (geologic) time scale and broad spatial scale, and localized or transient mechanical processes can influence their fields. We consider that the differences between the strain-rate and stress fields directly reflect information on fault dynamics during seismic cycles which determines the degree of fault coupling, regardless of specific areas such as a forearc. From this perspective, we will focus on the spatiotemporal changes

in actual data for the Japanese Islands with rich sets of observational data.

This study extends the results of Townend and Zoback (2006) using recent geodetic and seismological data, and systematically compares the strain-rate and stress fields across the Japanese Islands. In particular, the 2011 off the Pacific coast of Tohoku megathrust earthquake ($\sim M_w$ 9) impacted the eastern part of the Japanese Islands (e.g., Hasegawa et al. 2012; Becker et al. 2018), and was a key event in obtaining time-varying information of the azimuthal differences not available in the previous studies.

To estimate the strain-rate field, we use the surface displacement data of GEONET, a GNSS array by the Geospatial Information Authority of Japan (GSI), as in many previous studies (e.g., Sagiya et al. 2000; Nishimura et al. 2018; Fukahata et al. 2020). In recent years, several methods have been developed for calculating strain rates from surface displacement data that can take into account the spatial heterogeneity of station spacing (Shen et al. 2015; Sandwell and Wessel 2016; Okazaki et al. 2021). With the development of automatic polarity picking based on machine learning, focal mechanisms of smaller earthquakes can be estimated more accurately than before (Uchide 2020). Based on the above, we construct a dataset of geodetic strain-rate fields for the Japanese Islands with an original method to estimate an optimal hyperparameter for spatial smoothing and compare it with seismological stress fields in terms of azimuths of the maximum contraction. This quantitative dataset has wider temporal and spatial coverage than the previous studies (e.g., Townend and Zoback 2006; Matsumoto et al. 2015) and can serve as a basis for further research (statistical or physics-based simulation studies).

Estimation of geodetic strain-rate field

To obtain the strain-rate field, we first calculate the horizontal velocity vector for each GNSS observation point (GEONET station) from the F5 daily solution provided by GSI (Muramatsu et al. 2021), and then estimate the strain rates at grid points at 0.3-degree intervals on the Japanese Islands using a least-square method.

In particular, we calculate the horizontal velocity vectors for a total of 19 periods of 3 years from the average coordinates in February of GEONET stations: 1997–2000, 1998–2001, 1999–2002, 2000–2003, 2001–2004, 2002–2005, 2003–2006, 2004–2007, 2005–2008, 2006–2009, 2007–2010, 2008–2011 before the 2011 off the Pacific coast of Tohoku earthquake, and 2012–2015, 2013–2016, 2014–2017, 2015–2018, 2016–2019, 2017–2020, 2018–2021 after the 2011 off the Pacific coast of Tohoku earthquake. The coordinate offsets due to the GNSS antenna replacement and the coseismic displacement due to major earthquakes around the Japanese Islands (Table 1) are removed, where we chose them based on the criterion of a seismic intensity of 6 or 7 determined by the Japan Meteorological Agency. We compute the horizontal velocity vectors from the average coordinates starting in February of each year after removing outliers by Super Smoother (Friedman 1984), and transform them to the Eurasian plate reference frame based on International Terrestrial Reference System (ITRF) 2014 (Altamimi et al. 2016).

As an example, Fig. 1 shows the horizontal velocity vectors for the period from 2008 to 2011. Westward velocity is dominant due to the dual subduction of the Philippine

Table 1 Earthquakes of which coseismic displacement is removed

Date (JST)	Longitude, latitude [°]	Magnitude
May 13, 1997	130.303, 31.948	6.4
September 3, 1998	140.901, 39.806	6.2
July 1, 2000	139.194, 34.190	6.5
July 9, 2000	139.231, 34.212	6.1
July 15, 2000	139.242, 34.423	6.3
July 30, 2000	139.411, 33.971	6.5
August 18, 2000	139.241, 34.202	6.1
October 6, 2000	133.349, 35.274	7.3
March 24, 2001	132.694, 34.132	6.7
May 26, 2003	141.651, 38.821	7.1
September 26, 2003	144.078, 41.779	8.0
October 23, 2004	138.867, 37.292	6.8
October 27, 2004	139.033, 37.292	6.1
March 20, 2005	130.176, 33.739	7.0
August 16, 2005	142.278, 38.150	7.2
March 25, 2007	136.686, 37.221	6.9
July 16, 2007	138.609, 37.557	6.8
June 14, 2008	140.881, 39.030	7.2
August 11, 2009	138.499, 34.786	6.5
April 13, 2013	134.829, 34.419	6.3
November 22, 2014	137.891, 36.693	6.7
April 14, 2016	130.809, 32.742	6.5
April 15, 2016	130.778, 32.701	6.4
April 16, 2016	130.763, 32.755	7.3
June 16, 2016	140.987, 41.949	5.3
October 21, 2016	133.856, 35.380	6.6
December 28, 2016	140.574, 36.720	6.3
June 18, 2018	135.622, 34.844	6.1
September 6, 2018	142.007, 42.691	6.7
January 3, 2019	130.554, 33.027	5.1
February 21, 2019	142.003, 42.766	5.8
June 18, 2019	139.479, 38.608	6.7
February 13, 2021	141.698, 37.728	7.3

The longitude and latitude of hypocenters and magnitude are from the earthquake catalog provided by Japan Meteorological Agency

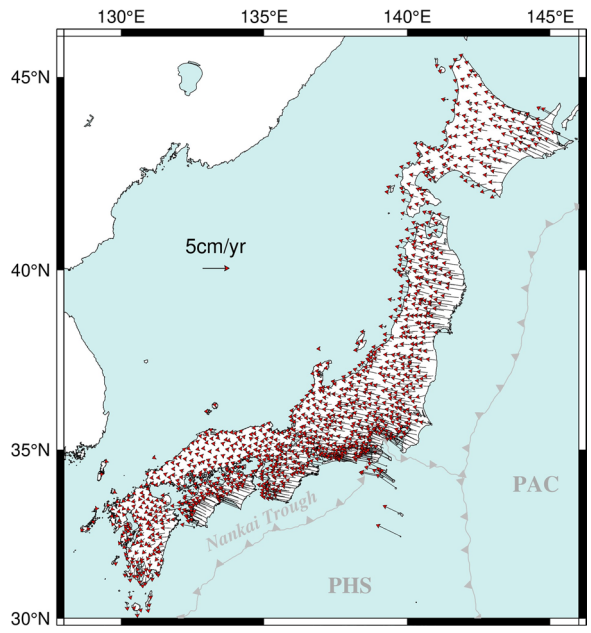

Fig. 1 Horizontal velocity vectors for the period from 2008 to 2011 (in February, before the 2011 off the Pacific coast of Tohoku earthquake). The vectors are transformed to the Eurasian plate reference frame based on ITRF 2014. "PHS" means the Philippine Sea plate and "PAC" does the Pacific plate. The ocean to the east and south of the Japanese Islands is the Pacific Ocean

Sea plate (PHS) and the Pacific plate (PAC) beneath the Japanese Islands.

The constitutive equation for the estimation of the strain-rate field follows previous studies (Shen et al. 1996, 2015). First, at each grid point, the observation equation $\boldsymbol{d} = \boldsymbol{G}\boldsymbol{m} + \boldsymbol{e}$ is constructed. Namely,

$$\boldsymbol{d} = \begin{pmatrix} V_x^i \\ V_y^i \end{pmatrix}, \tag{1}$$

$$\boldsymbol{G} = \begin{pmatrix} 1 & 0 & \Delta y^i & \Delta x^i & \Delta y^i & 0 \\ 0 & 1 & -\Delta x^i & 0 & \Delta x^i & \Delta y^i \end{pmatrix}, \tag{2}$$

$$\boldsymbol{m} = \begin{pmatrix} U_x \\ U_y \\ \omega \\ \tau_{xx} \\ \tau_{xy} \\ \tau_{yy} \end{pmatrix}, \tag{3}$$

$$\boldsymbol{e} = \begin{pmatrix} \varepsilon_x^i \\ \varepsilon_y^i \end{pmatrix}, \tag{4}$$

where V and ε are the horizontal velocity and residual (or error) at the observation point i (the subscripts x, y are the east–west and north–south components), U is the translational component, ω is the rotational component, and τ is the strain component at the grid point. The horizontal distance from the grid point to the observation point i is ΔR, and its east–west component is Δx and north–south component is Δy.

We compute the least-squares solution $\boldsymbol{m} = \left(\boldsymbol{G}^T \boldsymbol{W} \boldsymbol{G}\right)^{-1} \boldsymbol{G}^T \boldsymbol{W} \boldsymbol{d}$. The weight matrix $\boldsymbol{W}$ is a diagonal matrix satisfying

$$\mathrm{diag}(\boldsymbol{W}) = \exp\left(\frac{-\Delta R_i^2}{D^2}\right), \tag{5}$$

where D is the smoothing distance. We do not assume that D is the same for all grid points (Shen et al. 1996) because of the variability of the intervals between observation points in the GEONET array. Instead, we set D as the largest integer that satisfies the following criterion (Shen et al. 2015) for each grid point:

$$S = 2\sum_{i=1}^{n} \exp\left(\frac{-\Delta R_i^2}{D^2}\right), \tag{6}$$

$$\mathrm{int}(S) < W_t, \tag{7}$$

where n is the number of observation points used to estimate the strain-rate field at each grid point, and is assumed to be in the range of $\Delta R < 2.15D$. The factor 2.15 is based on the criterion of $\exp\left(-\Delta R_i^2/D^2\right) < 0.01$. W_t is a hyperparameter. Note that D depends on the observation periods for the same W_t. The method can reflect the changes in the density of the GNSS observation points by introducing the spatiotemporally variable D.

While the previous study using the GNSS network in southern California (Shen et al. 2015) tested several values of W_t and adopted $W_t = 24$ based on visual inspection for the strain-rate pattern, we originally estimate the optimal W_t with a new algorithm for the GEONET array in the Japanese Islands. Eight possible values of W_t are considered: 1, 4, 8, 12, 16, 20, 24, and 28. Using the horizontal velocity vectors of the forementioned 19 periods, we estimate the strain-rate field based on Eqs. (1)–(7) with the eight different W_t values. To determine the optimal W_t, the standard deviation σ of the residuals at each grid point is calculated as follows:

$$\sigma = \frac{\boldsymbol{e}^T \boldsymbol{W} \boldsymbol{e}}{2n - 6}, \tag{8}$$

where 2 is the number of components of the observed data (east–west and north–south), and 6 is the number of parameters of m. In this study, we consider that W_t with a smaller interquartile range (IQR) of σ is more appropriate because of the similar adequacy of the grid point representation.

We determine the optimal value of W_t after calculating σ for the strain-rate fields of the aforementioned 19 periods. Figure 2 summarizes the relation between IQR(σ) and W_t for the 19 periods, divided into 12 periods before the 2011 off the Pacific coast of Tohoku earthquake (Phase 1; 1997–2000 to 2008–2011 in February), 4 earlier periods of postseismic deformation of the 2011 off the Pacific coast of Tohoku earthquake (Phase 2; 2012–2015 to 2015–2018 in February), and 3 periods afterward (Phase 3; 2016–2019 to 2018–2021 in February). In Phase 1 before the 2011 off the Pacific coast of Tohoku earthquake, we find that $W_t = 12$ can reduce the overall IQR(σ). In Phase 2 immediately after the 2011 off the Pacific coast of Tohoku earthquake, $W_t = 4$ is the optimum, which may reflect the influence of the postseismic deformation of the 2011 off the Pacific coast of Tohoku earthquake (e.g., Ozawa et al. 2012; Suito 2017; Morikami and Mitsui 2020). In Phase 3, a few years later, the IQR(σ) are close to the minimum values at $W_t = 12$, as in Phase 1, probably due to the decay of the postseismic deformation. Therefore, we propose that the optimal W_t for the GEONET array in the Japanese Islands is 12 except immediately after the 2011 off the Pacific coast of Tohoku megathrust earthquake (as Phase 2). Besides, we do not consider that Phase 2 represented the characteristic decay time of the postseismic deformation of the 2011 off the Pacific coast of Tohoku earthquake. Because our analysis targeted the entire Japanese Islands, the transition between Phase 2 and Phase 3 might include other effects than the postseismic deformation of the 2011 off the Pacific coast of Tohoku earthquake, such as the occurrence of the M_w 7.0 2016 Kumamoto earthquake.

Figure 3 shows an example of the spatial distribution of the optimized smoothing distance D, which reflects the spatial heterogeneity of station spacing, for $W_t = 12$. Figure 4 presents examples of the estimated strain-rate fields. The fields of the dilatational strain rates ($\tau_{xx} + \tau_{yy}$) overall represent areal decrease due to the plate subduction beneath the Pacific ocean except for local strains such as those around volcanoes (e.g., Sagiya 2004). In addition, comparing the results of Phase 1 (1997–2000) and Phase 3 (2016–2019), the effects of the postseismic deformation of the 2011 off the Pacific coast of Tohoku earthquake perturb the strain fields along the Pacific coast (Fig. 4). There is a tendency for dilatation (areal increase) north of about 39° N and areal decrease south of about 39° N, indicating the north–south (along-strike) contrast in the postseismic deformation.

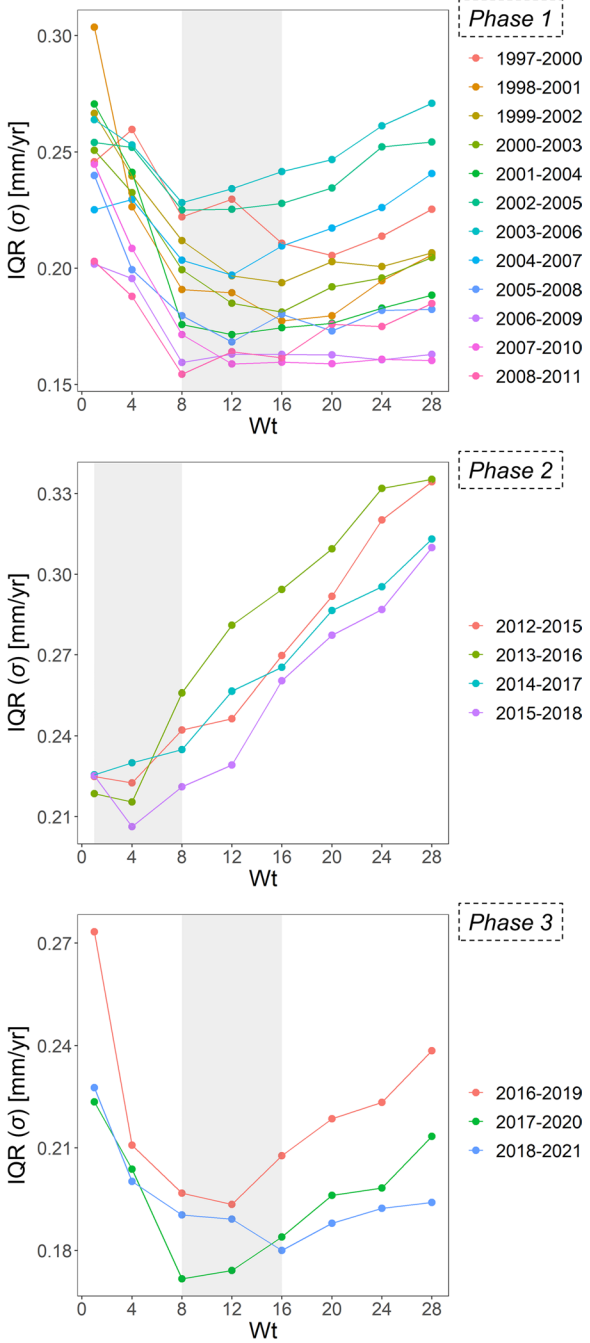

Fig. 2 Results of IQR(σ) and W_t for the 19 periods, in Phase 1 before the 2011 off the Pacific coast of Tohoku earthquake (top figure), Phase 2 immediately after the 2011 off the Pacific coast of Tohoku earthquake (center figure), and Phase 3 afterward (bottom figure). The gray shadings indicate W_t ranges with relatively small IQR (σ)

We compute the azimuth of the maximum contraction strain rate τ_{Hmax}, Az(τ_{Hmax}), as follows:

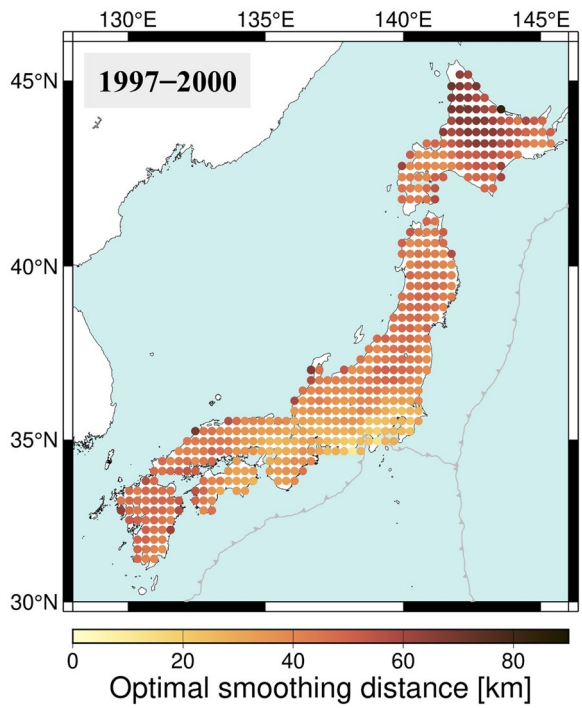

Fig. 3 An example of the spatial distribution of the optimal smoothing distance D during 1997–2000 in Phase 1 for $W_t = 12$, estimated from the GNSS data

$$\mathrm{Az}(\tau_{\mathrm{Hmax}}) = -0.5\mathrm{atan}\left(\frac{2\tau_{xy}}{(\tau_{xx} - \tau_{yy})}\right), \tag{9}$$

where the azimuth is a clockwise angle from the north. Additional file 1: Data S1 shows the estimation results of the strain rate fields for the 19 periods.

Comparison between azimuths of strain rate and stress

To estimate the azimuths of the maximum compressive stress (S_{Hmax}) for comparing those of the maximum contraction of geodetic strain rate (τ_{Hmax}), we use the earthquake focal mechanisms estimated by a previous study (Uchide 2020). That study was based on machine learning (neural network) for identifying the initial polarity of seismic waves, and succeeded in estimating far more mechanisms than before. The spatiotemporal range of the focal mechanism data is for the period from February 1, 2005, to February 28, 2015, for shallow depths less than 20 km, which corresponds to inland crustal earthquakes (Uchide 2020).

We calculate the azimuths of the maximum compressive stress (S_{Hmax}) using the plunge and azimuth angles of the t-, b-, and p-axes from the strike, dip, rake angles of focal mechanisms (Zoback 1992; Gasperini and Vannucci 2003; Kagan 2007). Next, from the calculated S_{Hmax} of each

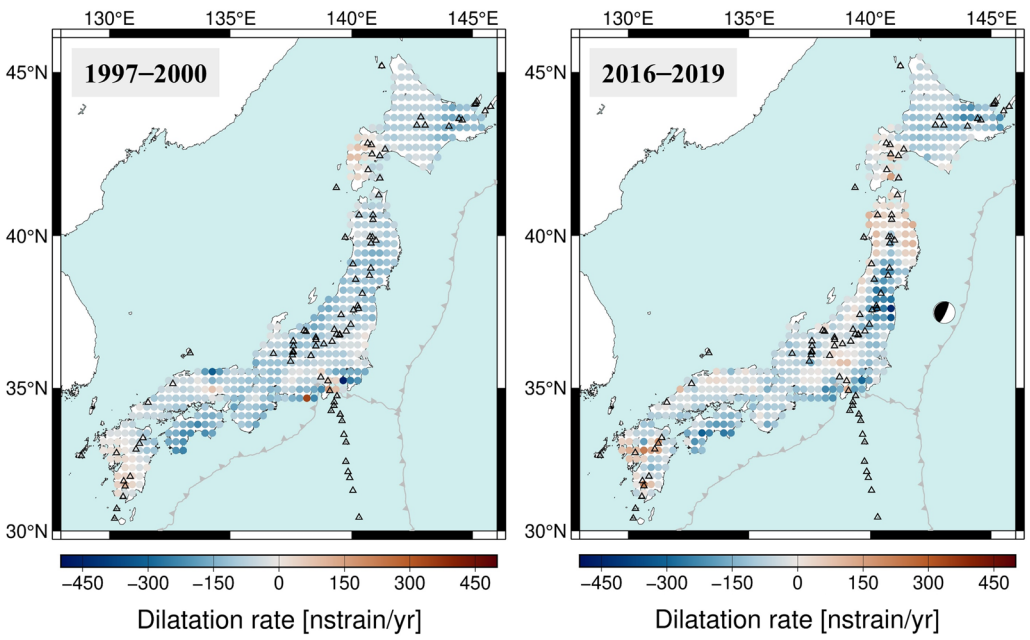

Fig. 4 Examples of the spatial distribution of the dilatational strain rates during 1997–2000 in Phase 1 (left figure) and during 2016–2019 in Phase 3 (right figure). The negative values represent areal decrease and the positive ones represent areal increase. The triangles show the Holocene volcanoes listed by the Global Volcanism Program (Smithsonian Institution 2022). The focal sphere in the right figure is the global centroid moment tensor solution of the 2011 off the Pacific coast of Tohoku earthquake (Nettles et al. 2011)

earthquake, we evaluate the S_{Hmax} values on the grid points used to estimate the strain-rate fields based on a simple weighted-average approach (e.g., Imanishi et al. 2019). A weight (W) for each focal mechanism is as follows:

$$W = \exp\left(\frac{-x^2}{\alpha^2}\right), \tag{10}$$

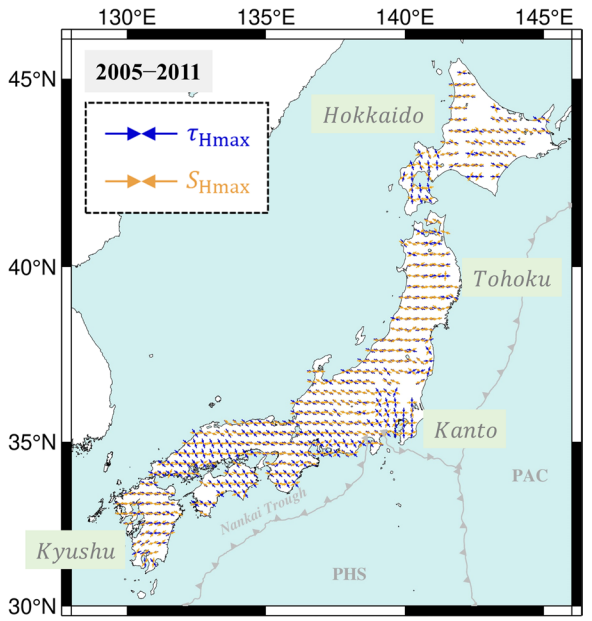

Fig. 5 Examples of the azimuths of the maximum contraction of geodetic strain rate τ_{Hmax} (blue arrows) and the maximum compressive stress S_{Hmax} (orange arrows) during 2005–2011 in Phase 1 before the 2011 off the Pacific coast of Tohoku earthquake. Hokkaido, Tohoku, Kanto, and Kyushu are the names of regions

where x is the epicentral distance from the grid point to the focal mechanism, and α is set to be equal to D at each grid point for the estimation of the strain-rate fields. We do not perform stress-tensor inversion as many previous studies about the comparison between strain and stress (e.g., Townend and Zoback 2006; Matsumoto et al. 2015; Noda et al. 2020; Yuasa et al. 2020), because this weighted-average approach can provide high spatial resolution in stress fields (e.g., Imanishi et al. 2019).

Figure 5 shows examples of the azimuths of the maximum contraction of geodetic strain rate (τ_{Hmax}), those of the maximum compressive stress (S_{Hmax}), during 2005–2011 in Phase 1. First, the azimuths of τ_{Hmax} are nearly east–west contraction in the Hokkaido (north of about 41.5° N) and Tohoku (north of about 37° N) regions of eastern Japan (except for the southwestern part of Hokkaido), reflecting the elastic coupling effect of the subduction of the Pacific plate (PAC). In the remaining region along the Pacific coast, the elastic coupling effect of the subduction of the Philippine Sea plate (PHS) seems dominant for the variable contraction. Second, the azimuths of S_{Hmax} appear to be nearly east–west direction with local exceptions and imply a widespread effect of the subduction of the Pacific plate (PAC), as was investigated by previous studies (e.g., Ukawa 1982; Seno 1999; Terakawa and Matsu'ura 2010). To clarify the differences in trends between the azimuths of τ_{Hmax} and S_{Hmax}, Fig. 6 shows the histogram of all the data in Fig. 5. While the distribution of the azimuths of τ_{Hmax} is biased greater than 90° (east–west direction), that of S_{Hmax} is approximately normally distributed around 90° (east–west direction). A maximum-likelihood estimation based on the normal

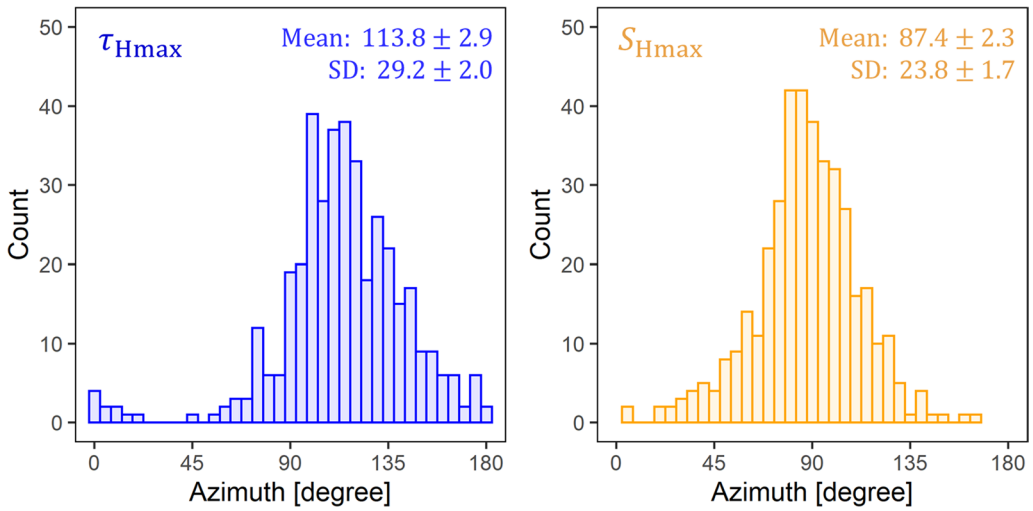

Fig. 6 Histogram of the azimuths of the maximum contraction of geodetic strain rate τ_{Hmax} (left figure) and the maximum compressive stress S_{Hmax} (right figure) during 2005–2011 in Phase 1 (the same as Fig. 5). The azimuth of the horizontal axis represents a clockwise angle from the north (defined in the range of 0 to 180°)

distribution model indicates that the mean and standard deviation (SD) of τ_{Hmax} are 113.8 ± 2.9 and 29.2 ± 2.0, respectively, and the mean and standard deviation (SD) of S_{Hmax} are 87.4 ± 2.3 and 23.8 ± 1.7, respectively, where the errors mean the 95% confidence intervals. According to the hypothesis that geodetic strain rates reflect temporal deformation, whereas earthquakes reflect averages of longer durations (e.g., Sbar 1983; Wang 2000), the differences in the azimuths may indicate the effect of the very long-term stable subduction (>40 Ma) of the Pacific plate (e.g., Harada and Hamano 2000) much longer than the Philippine Sea plate.

In Fig. 5, the azimuths of τ_{Hmax} and S_{Hmax} approximately match in the Hokkaido and Tohoku regions of eastern Japan (except for the southwestern part of Hokkaido), and around central Japan and the Kyushu region (south of about 34° N and west of about 132° E). On the other hand, in the southwestern part of Hokkaido, the Kanto region (south of about 37° N and east of about 139° E), and most of the areas along the Nankai Trough, the azimuths of τ_{Hmax} and S_{Hmax} differ evidently.

We will examine whether the spatial trends of the azimuths in each region varied with time. Additional file 2: Data S2 shows the comparative results of the strain rate and stress fields for periods of 2005–2011 in Phase 1 and 2016–2019 in Phase 3.

Spatiotemporal change of azimuthal difference

Figure 7 shows comparative histograms of the absolute azimuthal differences of τ_{Hmax} and S_{Hmax} before and after the 2011 off the Pacific coast of Tohoku earthquake (during 2005–2011 in Phase 1 and during 2016–2019 in Phase 3). Although there are no characteristic values of the azimuthal differences, we will focus on the value of 60° as a reference that τ_{Hmax} and S_{Hmax} are notably different. We select the value of 60° because there are obviously less data above 60° in the 2016–2019 histogram (Fig. 7).

Figure 8 shows the result for the Hokkaido and Tohoku regions. In these regions with the dominant elastic coupling effect of the subduction of the Pacific plate (PAC), the differences in the azimuths of τ_{Hmax} and S_{Hmax} were almost smaller than 60°. There are two exceptions as indicated in (1)–(2) below.

(1) One of the exceptions is that a large azimuthal shift occurred in the deep extension of the 2011 off the Pacific coast of Tohoku earthquake during 2016–2019 in Phase 3. The azimuths of τ_{Hmax} (strain rate) rather than S_{Hmax} (stress) rotated notably, closer to north–south contraction (on the other hand, east–west extension). This represented the post-seismic deformation of the 2011 off the Pacific coast of Tohoku earthquake (Meneses-Gutierrez and Sagiya 2016). Seismological stress may have lower response sensitivity to major earthquakes than geodetic strain rate, since the strength of fault tends to suppress earthquake occurrence.
(2) The other exception is that a large difference between the azimuths of τ_{Hmax} and S_{Hmax} in the southwestern part of Hokkaido was observed only

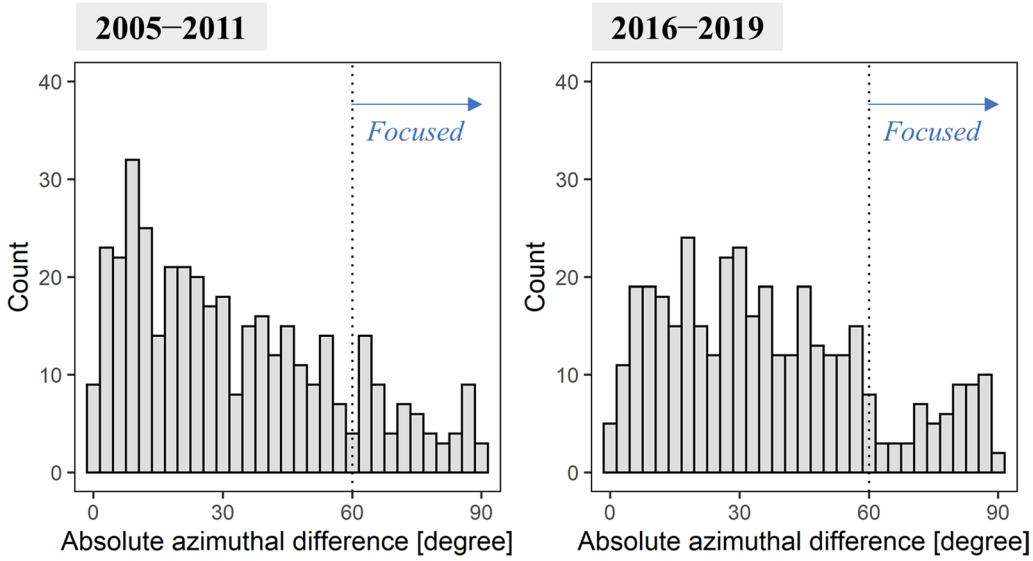

Fig. 7 Histogram of the absolute azimuthal differences of τ_{Hmax} and S_{Hmax} during 2005–2011 in Phase 1 before the 2011 off the Pacific coast of Tohoku earthquake (left figure) and during 2016–2019 in Phase 3 after the 2011 off the Pacific coast of Tohoku earthquake (right figure). We focus on cases with larger differences than 60°

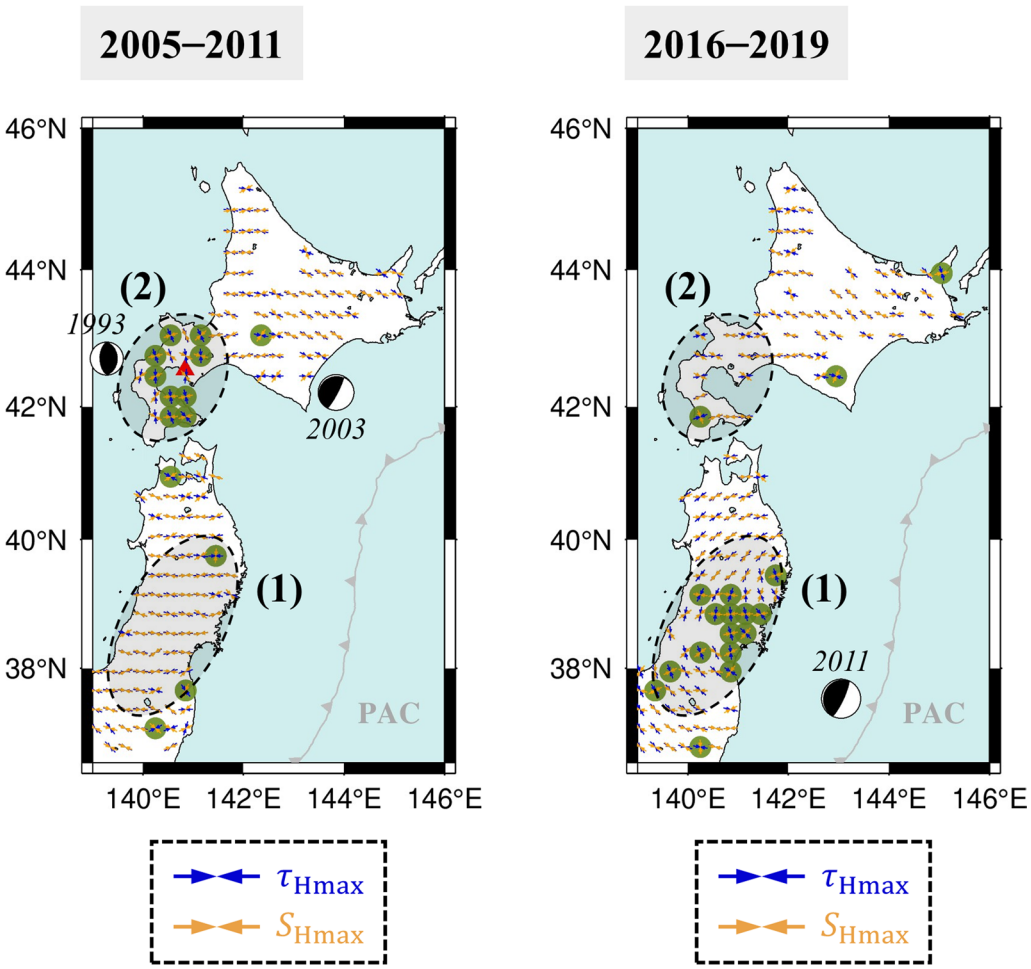

Fig. 8 Comparison between the azimuths of the maximum contraction of geodetic strain rate τ_{Hmax} (blue arrows) and the maximum compressive stress S_{Hmax} (orange arrows) before and after the 2011 off the Pacific coast of Tohoku earthquake (during 2005–2011 in Phase 1 and during 2016–2019 in Phase 3) for the Hokkaido and Tohoku regions. The green circles represent the grid points where the azimuths differ by more than 60°. (1) and (2) show areas of characteristic results. The red triangle shows the Usu volcano. The focal spheres in the left figure are the global centroid moment tensor solution (Ekström et al. 2012) of the 1993 Hokkaido Nansei-oki earthquake and the 2003 Tokachi-oki earthquake, and that in the right figure is the 2011 off the Pacific coast of Tohoku earthquake

for 2005–2011 in Phase 1. Especially the azimuths of τ_{Hmax} (strain rate) were closer to north–south contraction. Three events that had occurred before the investigation period (Phase 1) may be related. One is the 1993 Hokkaido Nansei-oki earthquake (M_w 7.7) off the west coast of Hokkaido (the epicenter was at 42.78° N, 139.18° E). The complex faulting of this earthquake caused evident viscoelastic relaxation (Ueda et al. 2003). It might have continued to fluctuate τ_{Hmax} in Phase 1 (2005–2011), although the earthquake had occurred more than 10 years before. Another is the 2000 eruption of Usu Volcano (42.54° N, 140.84° E) of which magma intrusion occurred at a subvertical fracture zone in the east–west direction (Jousset et al. 2003). The other is the 2003 Tokachi-oki earthquake (M_w 8.0) at the subduction plate interface off the south coast of Hokkaido (the epicenter was at 41.78° N, 143.86° E), whose postseismic deformation notably affected surface displacement fields in central to eastern Hokkaido (e.g., Itoh and Nishimura 2016). Viscoelastic relaxation due to both of the latter two events could fluctuate τ_{Hmax} in Phase 1 (2005–2011), but there remains a question whether they can account for the spatial scale of the large difference between the azimuths of τ_{Hmax} and S_{Hmax}.

Figure 9 shows the result for the Kanto region. Regardless of the observation period, before or

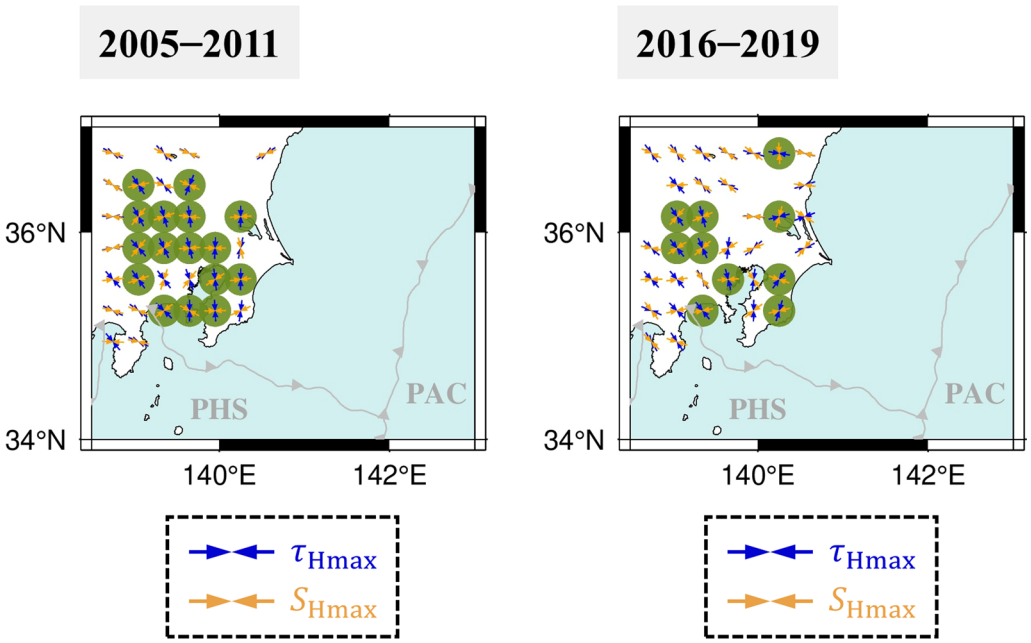

Fig. 9 Comparison between the azimuths of the maximum contraction of geodetic strain rate τ_{Hmax} (blue arrows) and the maximum compressive stress S_{Hmax} (orange arrows) for the Kanto region. The green circles represent the grid points where the azimuths differ by more than 60° as those in Fig. 8

after the 2011 off the Pacific coast of Tohoku earthquake, the azimuths of τ_{Hmax} (strain rate) tended to be closer to north–south contraction reflecting the oblique subduction of the Philippine Sea plate (PHS) in contrast to the azimuths of S_{Hmax} (stress) of nearly east–west compression probably due to the subduction of the Pacific plate (PAC). This region is a typical example for the different azimuths of τ_{Hmax} and S_{Hmax} because of the subduction of PHS and PAC from different angles. There occurred major interplate earthquakes ($\sim M_w$ 8) between PHS and the upper plate in 1923, 1703, and even earlier (e.g., Shimazaki et al. 2011). The relationship between the dynamics of fault slip during the seismic cycle of these recurrent Kanto earthquakes and the temporal evolution of the azimuthal difference between τ_{Hmax} and S_{Hmax} should be further studied in future from both theoretical and monitoring aspects.

Figure 10 shows the result for central to southwest Japan. The 2011 off the Pacific coast of Tohoku earthquake had little impact on this region. The following (3)–(5) show characteristic results:

(3) On the Pacific coast along the Nankai Trough, as in the Kanto region, the azimuths of τ_{Hmax} tended to differ from S_{Hmax} due to the (slightly) oblique subduction of PHS (Wang 2000). The obliqueness might cause margin-parallel compression defining a forearc sliver (e.g., Fitch 1972; Wang 2000), but this study did not find a clear boundary for the forearc sliver corresponding to a developed geologic structure (Median Tectonic Line). The relationship between the fault dynamics during the seismic cycle of the recurrent major earthquakes (Nankai-Tonankai-Tokai earthquakes) along the Nankai Trough (e.g., Ando 1975; Ishibashi 2004) and the temporal evolution of the azimuthal differences should be clarified from both theoretical and monitoring aspects. For example, the impacts of slow-slip events at the plate interface, some of which had spanned several years (Ozawa 2017), may become clearer with further monitoring.

(4) In central Japan, the differences in the azimuths of τ_{Hmax} (strain rate) and S_{Hmax} (stress) were almost smaller than 60° which were similar results of the previous study (Townend and Zoback 2006) that interpreted them as the mountain-building collision processes. We support this interpretation. Besides, the central Japan region includes the Niigata-Kobe Tectonic Zone with active inland earthquakes and high strain rates (Sagiya et al. 2000; Meneses-Gutierrez et al. 2018). The small azimuthal difference between τ_{Hmax} and S_{Hmax} may be related to the inelastic deformation of the lower crust or mantle

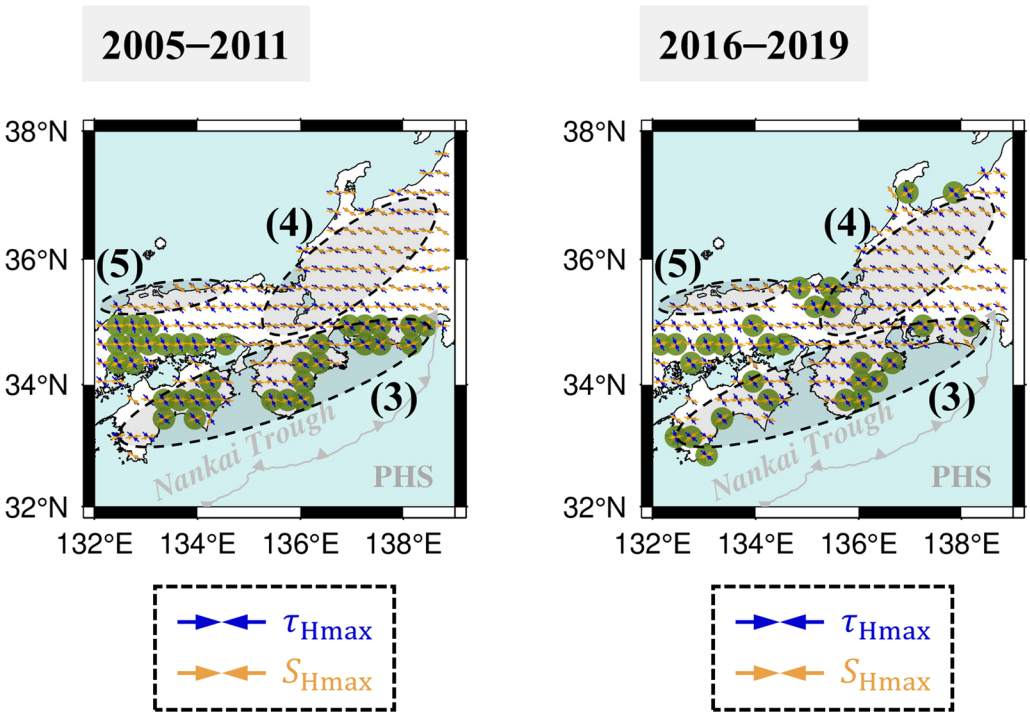

Fig. 10 Comparison between the azimuths of the maximum contraction of geodetic strain rate τ_{Hmax} (blue arrows) and the maximum compressive stress S_{Hmax} (orange arrows) for central to southwest Japan. The green circles represent the grid points where the azimuths differ by more than 60° as those in Fig. 8. (3)–(5) show areas of characteristic results

beneath the Niigata-Kobe Tectonic Zone (Iio et al. 2002; Yamasaki and Seno 2005) serving to bridge the azimuthal difference.

(5) On the back-arc side of the western Nankai Trough, as well as the central Japan region, the azimuths of τ_{Hmax} and S_{Hmax} were similar. This can be associated with the San-in Shear Zone with active inland earthquakes and high strain rates (Nishimura and Takada 2017), where inelastic deformation of the lower crust might also contribute (Meneses-Gutierrez and Nishimura 2020).

Note that, from a different perspective, the large differences in the azimuths of τ_{Hmax} (strain rate) and S_{Hmax} (stress) in the region between (4) and (5), after the 2011 off the Pacific coast of Tohoku earthquake (Fig. 10), may have another meaning such as a "connection" (part of a long-term integration) process between the Niigata-Kobe Tectonic Zone and the San-in Shear Zone.

Figure 11 shows the result for the Kyushu region (during 2005–2011 in Phase 1 and during 2016–2019 in Phase 3). The differences in the azimuths of τ_{Hmax} and S_{Hmax} were not pronounced, probably due to the relatively weak coupling of the subduction of the PHS (e.g., Loveless and Meade 2016). Apart from the subduction process of PHS, the Beppu-Shimabara graben area in central Kyushu has been spreading in a north–south direction in both geodetic and seismological sense (Matsumoto et al. 2015; Mochizuki and Mitsui 2016). The results of this study are consistent with the spreading process. Effects of the 2016 Kumamoto earthquake (M_w 7.0), whose epicenter was at 32.75° N, 130.76° E, have not been pronounced. In addition, active volcanoes such as Sakurajima, Kirishima, Aso, and Unzen should affect the azimuths locally.

On the whole, the differences in the azimuths of the maximum contraction of geodetic strain rate (τ_{Hmax}) and those of the maximum compressive stress (S_{Hmax}) well corresponded to regional seismotectonics for the Japanese Islands, regardless of specific areas such as a forearc. While they probably reflected the past deformation history in each region, they may also be related to the spatially heterogeneous inelastic rheology of rocks (e.g., Meneses-Gutierrez et al. 2018; Becker et al. 2018; Yuasa et al. 2020). Further interesting results on those details can be obtained by estimating offshore strain-rate fields based on seafloor crustal deformation data (e.g., Yokota et al. 2018). In addition, we should note that there must be many hidden faults that have not hosted earthquakes during the observation periods, and the stresses

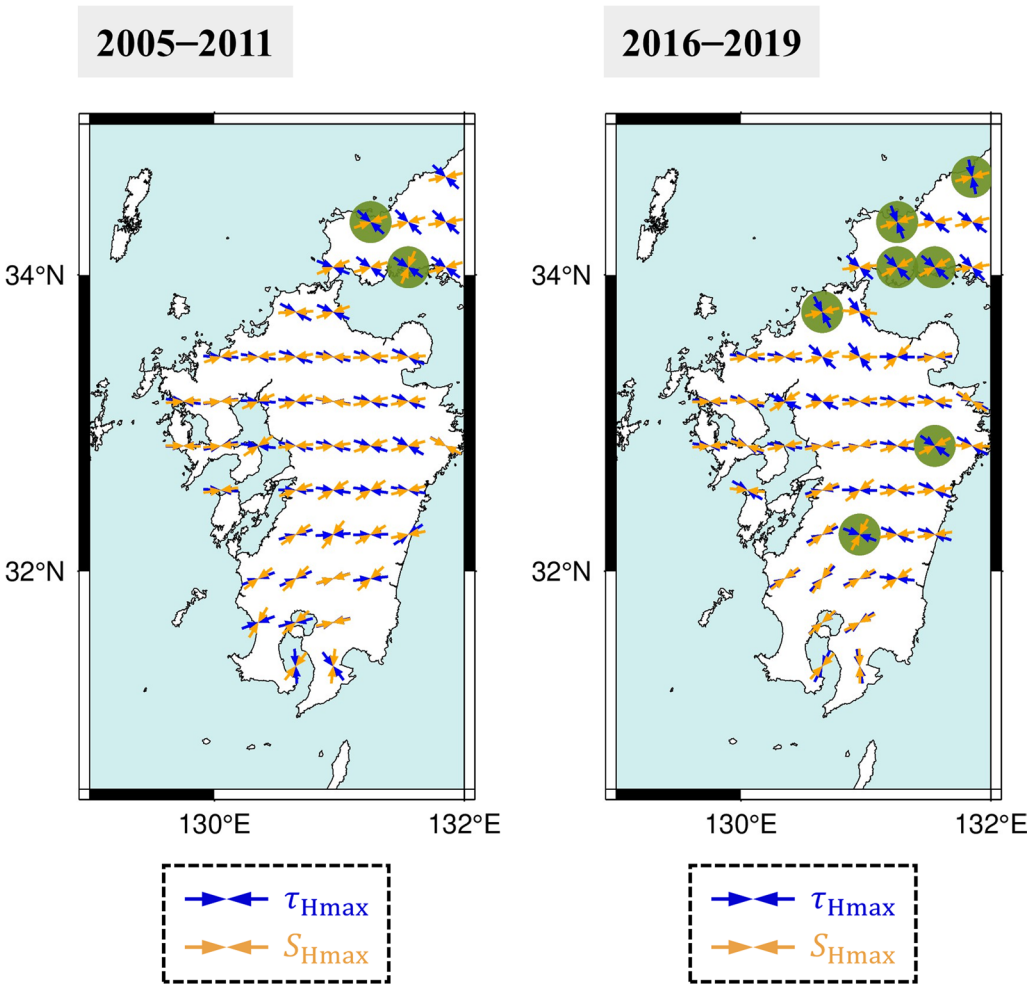

Fig. 11 Comparison between the azimuths of the maximum contraction of geodetic strain rate τ_{Hmax} (blue arrows) and the maximum compressive stress S_{Hmax} (orange arrows) for the Kyushu region. The green circles represent the grid points where the azimuths differ by more than 60° as those in Fig. 8

associated with such earthquakes have not been considered. In any case, we obtained clear evidence that the geophysical monitoring captured the time-varying information of the azimuthal differences in the strain rates and the stress, related to seismic cycles (and several surface phenomena).

The importance of our quantitative azimuthal differences which have wider temporal and spatial coverage than the previous studies (e.g., Townend and Zoback 2006; Matsumoto et al. 2015) is that they reflected information on fault dynamics during earthquake cycles. Correlating the azimuthal differences with other parameters, or comparing them with physics-based simulations, may inform us of the current conditions during seismic cycles on both interplate and inland faults (e.g., Loveless and Meade 2010; Nishimura et al. 2018).

Conclusion

We estimated the spatiotemporal variation of the strain-rate fields for the Japanese Islands, using an original method to estimate the optimal hyperparameter W_t for spatial smoothing. We made a direct comparison by taking the differences between the azimuths of the maximum contraction of geodetic strain rate (τ_{Hmax}) and those of the maximum compressive stress (S_{Hmax}) at the same grid points. The overall results truly reflected regional seismotectonics. On the other hand, a short-term effect of the postseismic deformation of the 2011 off the Pacific coast of Tohoku earthquake was also detected. Our quantitative dataset has wider spatiotemporal coverage than the previous studies and can contribute to further research.

Abbreviations
GNSS: Global Navigation Satellite System; GSI: Geospatial Information Authority of Japan.

Supplementary Information

The online version contains supplementary material available at https://doi.org/10.1186/s40623-022-01701-7.

Additional file 1: Data S1. (e.g., 1997-2000.out) The estimation results of the strain rate fields for the 19 periods in Fig. 2. We set $W_t = 12$ for Phase 1 (1997–2000 to 2008–2011) and Phase 3 (2016–2019 to 2018–2021), and $W_t = 4$ for Phase 2 (2012–2015 to 2015–2018). The first column of data represents the longitude of the grid point, the second does the latitude, the third does the optimized smoothing distance *D* [km], the fourth does the dilatational strain rate [nstrain/year], the fifth does the maximum shear strain rate [nstrain/year], and the sixth does the azimuth of the maximum contraction of strain rate τ_{Hmax} [°].

Additional file 2: Data S2. (e.g., 2005-2011diff.out) The comparative results of the strain rate and stress fields for the periods of 2005–2011 in Phase 1 and 2016–2019 in Phase 3. The first column of data represents the longitude of the grid point, the second does the latitude, the third does the optimized smoothing distance *D* [km], the fourth does the dilatational strain rate [nstrain/year], the fifth does the maximum shear strain rate [nstrain/year], the sixth does the azimuth of the maximum contraction of strain rate τ_{Hmax} [°], the seventh does the azimuth of the maximum compressive stress S_{Hmax} [°], the eighth does the number of earthquakes, and the ninth does the absolute difference between the azimuths of τ_{Hmax} and S_{Hmax} [°].

Acknowledgements
We thank the Geospatial Information Authority of Japan and the Japan Meteorological Agency for providing the data. We are grateful to Xanthos Papanikolaou and Yukitoshi Fukahata for discussion. Constructive comments by Jack Loveless, Takeshi Sagiya, and an anonymous reviewer improved this manuscript. We acknowledge support from the Japan Society for the Promotion of Science (JSPS) KAKENHI, Grant Numbers JP19K04036 and JP21H05205. The author Issei Kosugi received the Seto Prize of the Geodetic Society of Japan and this study was supported by the award.

Author contributions
IK conceived and conducted the data analyses. YM discussed the results and wrote the paper. All authors read and approved the final manuscript.

Funding
This study was supported by the Japan Society for the Promotion of Science (JSPS) KAKENHI, Grant Numbers JP19K04036 and JP21H05205.

Availability of data and materials
Please contact the author for data requests.

Declarations

Ethics approval and consent to participate
Not applicable.

Consent for publication
Not applicable.

Competing interests
The authors declare no competing financial interests.

Received: 15 March 2022 Accepted: 29 August 2022
Published online: 13 September 2022

References

Altamimi Z, Rebischung P, Métivier L, Collilieux X (2016) ITRF2014: a new release of the International Terrestrial Reference Frame modeling nonlinear station motions. J Geophys Res 121:6109–6131. https://doi.org/10.1002/2016JB013098
Ando M (1975) Source mechanisms and tectonic significance of historical earthquakes along the Nankai Trough, Japan. Tectonophysics 27:119–140. https://doi.org/10.1016/0040-1951(75)90102-X
Becker TW, Hashima A, Freed AM, Sato H (2018) Stress change before and after the 2011 M9 Tohoku-oki earthquake. Earth Planet Sci Lett 504:174–184. https://doi.org/10.1016/j.epsl.2018.09.035
Ekström G, Nettles M, Dziewoński AM (2012) The global CMT project 2004–2010: centroid-moment tensors for 13,017 earthquakes. Phys Earth Planet Int 200–201:1–9. https://doi.org/10.1016/j.pepi.2012.04.002
Fitch TJ (1972) Plate convergence, transcurrent faults and internal deformation adjacent to Southeast Asia and the western Pacific. J Geophys Res 77:4432–4460
Friedman JH (1984) A variable span smoother. Tech Rep Stanford Univ 5
Fukahata Y, Meneses-Gutierrez A, Sagiya T (2020) Detection of plastic strain using GNSS data of pre- and post-seismic deformation of the 2011 Tohoku-oki earthquake. Earth Planets Space 72:18. https://doi.org/10.1186/s40623-020-1144-1
Gasperini P, Vannucci G (2003) FPSPACK: a package of FORTRAN subroutines to manage earthquake focal mechanism data. Comp Geosci 29:893–901. https://doi.org/10.1016/S0098-3004(03)00096-7
Harada Y, Hamano Y (2000) Recent progress on the plate motion relative to hotspots. In: Richards MA, Gordon RG, van der Hilst RD (eds) The history and dynamics of global plate motions. American Geophysical Union, Washington, pp 327–338
Hasegawa A, Yoshida K, Asano Y et al (2012) Change in stress field after the 2011 great Tohoku-Oki earthquake. Earth Planet Sci Lett 355–356:231–243. https://doi.org/10.1016/j.epsl.2012.08.042
Heki K, Miyazaki S (2001) Plate convergence and long-term crustal deformation in Central Japan. Geophys Res Lett 28:2313–2316. https://doi.org/10.1029/2000GL012537
Henry P, Mazzotti S, Le Pichon X (2001) Transient and permanent deformation of central Japan estimated by GPS 1. Interseismic loading and subduction kinematics. Earth Planet Sci Lett 184:443–453. https://doi.org/10.1016/S0012-821X(00)00335-6
Iio Y, Sagiya T, Kobayashi Y, Shiozaki I (2002) Water-weakened lower crust and its role in the concentrated deformation in the Japanese Islands. Earth Planet Sci Lett 203:245–253. https://doi.org/10.1016/S0012-821X(02)00879-8
Imanishi K, Uchide T, Ohtani M, Matsushita R, Nakai M (2019) Construction of the crustal stress map in the Kanto region, central Japan. Bull Geol Surv Japan 70(3):273–298 (**In Japanese with English abstract**)
Ishibashi K (2004) Status of historical seismology in Japan. Ann Geophys 47:339–368
Itoh Y, Nishimura T (2016) Characteristics of postseismic deformation following the 2003 Tokachi-oki earthquake and estimation of the viscoelastic structure in Hokkaido, northern Japan. Earth Planets Space 68:156. https://doi.org/10.1186/s40623-016-0533-y
Jousset P, Mori H, Okada H (2003) Elastic models for the magma intrusion associated with the 2000 eruption of Usu Volcano, Hokkaido, Japan. J Vol Geotherm Res 125:81–106. https://doi.org/10.1016/S0377-0273(03)00090-8
Kagan YY (2007) Simplified algorithms for calculating double-couple rotation. Geophys J Int 171:411–418. https://doi.org/10.1111/j.1365-246X.2007.03538.x
Loveless JP, Meade BJ (2010) Geodetic imaging of plate motions, slip rates, and partitioning of deformation in Japan. J Geophys Res 115:B02410. https://doi.org/10.1029/2008JB006248
Loveless JP, Meade BJ (2016) Two decades of spatiotemporal variations in subduction zone coupling offshore Japan. Earth Planet Sci Lett 436:19–30. https://doi.org/10.1016/j.epsl.2015.12.033
Matsumoto S, Nakao S, Ohkura T et al (2015) Spatial heterogeneities in tectonic stress in Kyushu, Japan and their relation to a major shear zone. Earth Planets Space 67:172. https://doi.org/10.1186/s40623-015-0342-8

Mazzotti S, Le Pichon X, Henry P, Miyazaki S-I (2000) Full interseismic locking of the Nankai and Japan-west Kurile subduction zones: an analysis of uniform elastic strain accumulation in Japan constrained by permanent GPS. J Geophys Res 105:13159–13177. https://doi.org/10.1029/2000JB900060
Mazzotti S, Henry P, Le Pichon X (2001) Transient and permanent deformation of central Japan estimated by GPS 2. Strain partitioning and arc–arc collision. Earth Planet Sci Lett 184:455–469. https://doi.org/10.1016/S0012-821X(00)00336-8
Meneses-Gutierrez A, Nishimura T (2020) Inelastic deformation zone in the lower crust for the San-in Shear Zone, Southwest Japan, as observed by a dense GNSS network. Earth Planets Space 72:10. https://doi.org/10.1186/s40623-020-1138-z
Meneses-Gutierrez A, Sagiya T (2016) Persistent inelastic deformation in central Japan revealed by GPS observation before and after the Tohoku-oki earthquake. Earth Planet Sci Lett 450:366–371. https://doi.org/10.1016/j.epsl.2016.06.055
Meneses-Gutierrez A, Sagiya T, Sekine S (2018) Crustal deformation process in the mid-Niigata region of the Niigata-Kobe Tectonic Zone as observed by dense GPS network before, during, and after the Tohoku-Oki Earthquake. J Geophys Res 123:6072–6085. https://doi.org/10.1029/2018JB015567
Mochizuki K, Mitsui Y (2016) Crustal deformation model of the Beppu-Shimabara graben area, central Kyushu, Japan, based on inversion of three-component GNSS data in 2000–2010. Earth Planets Space 68:177. https://doi.org/10.1186/s40623-016-0550-x
Morikami S, Mitsui Y (2020) Omori-like slow decay ($p < 1$) of postseismic displacement rates following the 2011 Tohoku megathrust earthquake. Earth Planets Space 72:37. https://doi.org/10.1186/s40623-020-01162-w
Muramatsu H, Takamatsu N, Abe S, Furuya T, Kato C, Ohno K, Hatanaka Y, Kakiage Y, Ohashi K (2021) Updating daily solution of CORS in Japan using new GEONET 5th analysis strategy. J Geogr Surv Inst 134 **(In Japanese)**
Nettles M, Ekstrom G, Koss HC (2011) Centroid-moment-tensor analysis of the 2011 off the Pacific coast of Tohoku Earthquake and its larger foreshocks and aftershocks. Earth Planets Space 63:519–523
Nishimura T, Takada Y (2017) San-in shear zone in southwest Japan, revealed by GNSS observations. Earth Planets Space 69:85. https://doi.org/10.1186/s40623-017-0673-8
Nishimura T, Yokota Y, Tadokoro K, Ochi T (2018) Strain partitioning and interplate coupling along the northern margin of the Philippine Sea plate, estimated from Global Navigation Satellite System and Global Positioning System-Acoustic data. Geosphere 14:535–551. https://doi.org/10.1130/GES01529.1
Noda A, Saito T, Fukuyama E et al (2020) The 3-D spatial distribution of shear strain energy changes associated with the 2016 Kumamoto earthquake sequence, southwest Japan. Geophys Res Lett 47:e2019GL086369. https://doi.org/10.1029/2019GL086369
Okazaki T, Fukahata Y, Nishimura T (2021) Consistent estimation of strain-rate fields from GNSS velocity data using basis function expansion with ABIC. Earth Planets Space 73:153. https://doi.org/10.1186/s40623-021-01474-5
Ozawa S (2017) Long-term slow slip events along the Nankai trough subduction zone after the 2011 Tohoku earthquake in Japan. Earth Planets Space 69:56. https://doi.org/10.1186/s40623-017-0640-4
Ozawa S, Nishimura T, Munekane H et al (2012) Preceding, coseismic, and postseismic slips of the 2011 Tohoku earthquake, Japan. J Geophys Res. https://doi.org/10.1029/2011JB009120
Sagiya T (2004) A decade of GEONET: 1994–2003—the continuous GPS observation in Japan and its impact on earthquake studies. Earth Planets Space 56:29–41. https://doi.org/10.1186/BF03353077
Sagiya T, Miyazaki S, Tada T (2000) Continuous GPS array and present-day crustal deformation of Japan. Pure Appl Geophys 157:2303–2322
Sandwell DT, Wessel P (2016) Interpolation of 2-D vector data using constraints from elasticity. Geophys Res Lett 43:10703–10709. https://doi.org/10.1002/2016GL070340
Sbar ML (1983) An explanation for contradictory geodetic strain and fault plane solution data in western North America. Geophys Res Lett 10:177–180. https://doi.org/10.1029/GL010i003p00177
Seno T (1999) Syntheses of the regional stress fields of the Japanese islands. Isl Arc 8:66–79. https://doi.org/10.1046/j.1440-1738.1999.00225.x
Shen Z-K, Jackson DD, Ge BX (1996) Crustal deformation across and beyond the Los Angeles basin from geodetic measurements. J Geophys Res 101:27957–27980. https://doi.org/10.1029/96JB02544
Shen Z, Wang M, Zeng Y, Wang F (2015) Optimal interpolation of spatially discretized geodetic data. Bull Seis Soc Am 105:2117–2127. https://doi.org/10.1785/0120140247
Shimazaki K, Kim HY, Chiba T, Satake K (2011) Geological evidence of recurrent great Kanto earthquakes at the Miura Peninsula. Japan J Geophys Res 116:B12408. https://doi.org/10.1029/2011JB008639
Smithsonian Institution (2022) Global Volcanism Program. https://volcano.si.edu/. Accessed 2 May 2022
Suito H (2017) Importance of rheological heterogeneity for interpreting viscoelastic relaxation caused by the 2011 Tohoku-Oki earthquake. Earth Planets Space 69:21. https://doi.org/10.1186/s40623-017-0611-9
Terakawa T, Matsu'ura M (2010) The 3-D tectonic stress fields in and around Japan inverted from centroid moment tensor data of seismic events. Tectonics 29:TC6008. https://doi.org/10.1029/2009TC002626
Townend J, Zoback MD (2006) Stress, strain, and mountain building in central Japan. J Geophys Res 111:B03411. https://doi.org/10.1029/2005JB003759
Uchide T (2020) Focal mechanisms of small earthquakes beneath the Japanese islands based on first-motion polarities picked using deep learning. Geophys J Int 223:1658–1671. https://doi.org/10.1093/gji/ggaa401
Ueda H, Ohtake M, Sato H (2003) Postseismic crustal deformation following the 1993 Hokkaido Nansei-oki earthquake, northern Japan: evidence for a low-viscosity zone in the uppermost mantle. J Geophys Res 108:B3. https://doi.org/10.1029/2002JB002067
Ukawa M (1982) Lateral stretching of the Philippine Sea Plate subducting along the Nankai-Suruga Trough. Tectonics 1:543–571. https://doi.org/10.1029/TC001i006p00543
Wang K (2000) Stress-strain paradox, plate coupling, and forearc seismicity at the Cascadia and Nankai subduction zones. Tectonophysics 319:321–338. https://doi.org/10.1016/S0040-1951(99)00301-7
Yamasaki T, Seno T (2005) High strain rate zone in central Honshu resulting from the viscosity heterogeneities in the crust and mantle. Earth Planet Sci Lett 232:13–27. https://doi.org/10.1016/j.epsl.2005.01.015
Yokota Y, Ishikawa T, Watanabe S (2018) Seafloor crustal deformation data along the subduction zones around Japan obtained by GNSS-A observations. Sci Data 5:180182. https://doi.org/10.1038/sdata.2018.182
Yuasa Y, Matsumoto S, Nakao S et al (2020) Inelastic strain rate and stress fields in and around an aseismic zone of Kyushu Island, Japan, inferred from seismic and GNSS data. Geophys J Int 221:289–304. https://doi.org/10.1093/gji/ggaa008
Zoback ML (1992) First- and second-order patterns of stress in the lithosphere: The World Stress Map Project. J Geophys Res 97:11703–11728. https://doi.org/10.1029/92JB00132

Publisher's Note